AD-A078 135 NAVAL RESEARCH LAB WASHINGTON DC F/G 18/11
MONTE CARLO METHODS FOR NEUTRON FLUX CALCULATIONS IN A PRESSURI--ETC(U)
UNCLASSIFIED NOV 79 R A LINDGREN , M ROSEN , A I NAMENSON NRL-MR-4115 NL

1 OF 1
AD A078135

END
DATE FILMED
1-80
DDC

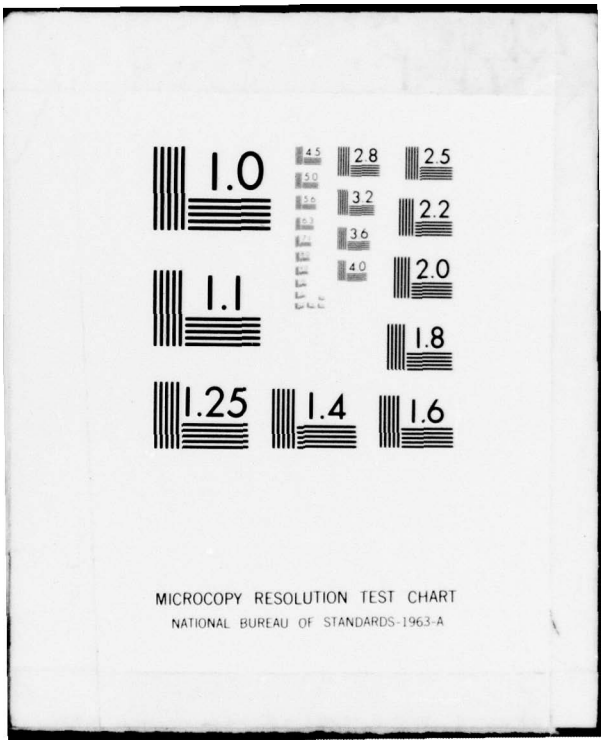
1.0
1.1
1.25
1.4
1.6
1.8
2.0
2.2
2.5
2.8
3.2
3.6
4.0
4.5
5.0
MICROCOPY RESOLUTION TEST CHART
NATIONAL BUREAU OF STANDARDS-1963-A

NRL Memorandum Report 4115

Monte Carlo Methods for Neutron Flux Calculations in a Pressurized Light Water Power Reactor Using Morse-CG •

R. A. LINDGREN

Nuclear Physics Group
University of Massachusetts
Amherst, Massachusetts

AND

M. ROSEN AND A. I. NAMENSON

Radiation-Matter Interactions Branch
Radiation Technology Division

27 November 27, 1979

RR012041

RR012041

NAVAL RESEARCH LABORATORY
Washington, D.C.

SECURITY CLASSIFICATION OF THIS PAGE (When Data Entered)

REPORT DOCUMENTATION PAGE		READ INSTRUCTIONS BEFORE COMPLETING FORM
1. REPORT NUMBER NRL Memorandum Report 4115	2. GOVT ACCESSION NO.	3. RECIPIENT'S CATALOG NUMBER
4. TITLE (and Subtitle) MONTE CARLO METHODS FOR NEUTRON FLUX CALCULATIONS IN A PRESSURIZED LIGHT WATER POWER REACTOR USING MORSE-CG		5. TYPE OF REPORT & PERIOD COVERED Interim report on a continuing NRL problem. 6. PERFORMING ORG. REPORT NUMBER
7. AUTHOR(s) R. A. Lindgren*, M. Rosen and A. I. Namenson		8. CONTRACT OR GRANT NUMBER(s)
9. PERFORMING ORGANIZATION NAME AND ADDRESS Naval Research Laboratory Washington, DC 20375		10. PROGRAM ELEMENT, PROJECT, TASK AREA & WORK UNIT NUMBERS NRL Problem H01-80 RR012-01-41
11. CONTROLLING OFFICE NAME AND ADDRESS		12. REPORT DATE November 27, 1979 13. NUMBER OF PAGES 49
14. MONITORING AGENCY NAME & ADDRESS(if different from Controlling Office)		15. SECURITY CLASS. (of this report) UNCLASSIFIED 15a. DECLASSIFICATION/DOWNGRADING SCHEDULE

16. DISTRIBUTION STATEMENT (of this Report)

Approved for public release; distribution unlimited.

17. DISTRIBUTION STATEMENT (of the abstract entered in Block 20, if different from Report)

18. SUPPLEMENTARY NOTES

*Nuclear Physics Group, University of Massachusetts, Amherst, Massachusetts

This work was supported in part by the U.S. Nuclear Regulatory Commission under Contract Number AT(49-24)0348.

19. KEY WORDS (Continue on reverse side if necessary and identify by block number)

Fast neutron flux
Fast neutron spectra
Monte Carlo methods
Power reactors
Flux estimators
Importance sampling
Biasing

20. ABSTRACT (Continue on reverse side if necessary and identify by block number)

Various methods of optimizing Monte Carlo calculations of fast neutron flux and spectra in a pressurized light water reactor are investigated using the code MORSE. Results in slab and cylindrical geometry are compared with those of the code ANISN.

DD FORM 1 JAN 73 1473 EDITION OF 1 NOV 65 IS OBSOLETE
S/N 0102-014-6601

SECURITY CLASSIFICATION OF THIS PAGE (When Data Entered)

Table of Contents

MONTE CARLO METHODS FOR NEUTRON FLUX CALCULATIONS IN A PRESSURIZED LIGHT WATER POWER REACTOR USING MORSE-CG

I. INTRODUCTION

The fast neutron flux (E_n >1.0 MeV) and neutron energy spectra in the core midplane of a typical Oconee class pressurized light water power reactor have been calculated using the Monte Carlo computer code MORSE[1] with combinatorial geometry.

The purpose of the calculation was three fold: (1) to compare fast neutron flux in the core midplane of a nuclear reactor using a one-dimensional slab model as calculated with the code MORSE with that calculated[2] using the discrete ordinates code ANISN[3]; (2) to compare fast neutron flux results in slab and cylindrical models; and (3) to investigate the effect on neutron flux results of using different flux estimators.

Note: Manuscript submitted September 20, 1979.

The comparison between MORSE and ANISN using the slab model was investigated both to use as a benchmark calculation and to check the accuracy of ANISN against MORSE in a reactor geometry situation. ANISN solves the Boltzman transport equation in a discretized space with the method of finite differences, while MORSE solves the Boltzman transport equation in a continuous space using a Monte Carlo method. Although these two methods have been compared previously for simple homogenous slabs, the accuracy of ANISN when applied to amultiple-slab reactor geometry has not been checked in detail. Comparison between the slab and cylindrical models was also made.

In Monte Carlo type calculations, it is generally of some concern as to which estimator to use. An estimator is generally selected that will minimize the number of histories needed to attain a given statistical accuracy. It is, therefore, useful to compare fast neutron flux results in the slab model using various types of estimators. For the slab and cylindrical geometries, the only flux estimators we seriously considered were the boundary crossing estimator and the next event uncollided flux estimator. We have therefore compared results for these two estimators, but also used the collision density and track length per unit volume estimators[4] as checks.

The slab geometry and neutron source parameters used to describe the reactor are discussed in detail in Section II. Section III is a discussion of the biasing of the sampling of the neutron source energy and spatial distributions in the reactor core. In addition path-length stretching, energy biasing at the collision site, Russian roulette, splitting, and angle biasing are discussed there. Various neutron flux estimators are discussed in Section IV and the cylindrical modeling of the reactor in Section V. A discussion of the results of the fast neutron flux and neutron energy spectra calculated by MORSE and ANISN are given in Section VI.

II. MORSE MONTE CARLO CALCULATION IN THE SLAB MODEL

A. Composition and dimensions of reactor components

The characteristics of the reactor in this calculation were typical of Babcock and Wilcox Oconee class power reactors.[2] Neutron flux and spectrum calculations using ANISN have been performed[2] by Babcock and Wilcox using these reactor parameters and the cross section library CASK.[5]

In the slab model each component or region of the reactor is treated as a infinite slab with the normal to the surface in the Z direction as shown in Fig. 1. For the MORSE calculation the size of the slab in the X and Y direction was actually taken to be 20,000 cm,

which is infinite for all practical purposes. The exact dimensions of each slab is given in Table 1. The elemental composition, and atomic densities in each region are given in Table 2. The atomic densities in the reactor core were determined assuming the core is a homogeneous mixture.

B. Core power distribution function

The relative core power distribution was obtained from criticality calculations by Babcock and Wilcox using the computer codes[6,7] PDQ-5 and Harmony. In the slab model the source strength is proportional to the product of a relative power distribution function P(Z), which is invariant under translations in the X or Y direction and a neutron energy distribution function $\chi(E)$. We assume that source neutrons are emitted isotropically. The function P(Z) is given as a discrete set of average values on a set of intervals in the core region and are tabulated in Table 3 (together with the relative power density). The energy distribution function $\chi(E)$ is similarly defined on a discrete set of energy intervals or groups. The cross section library used in the calculation is CASK,[(4)] a 40 group coupled neutron and gamma-ray cross-section data set (22 neutron and 18 gamma-ray groups). We only made use of the 14 highest energy neutron groups since we are interested in fast flux only. The function χ is tabulated in Table 4. The neutron source strength function can then be written as

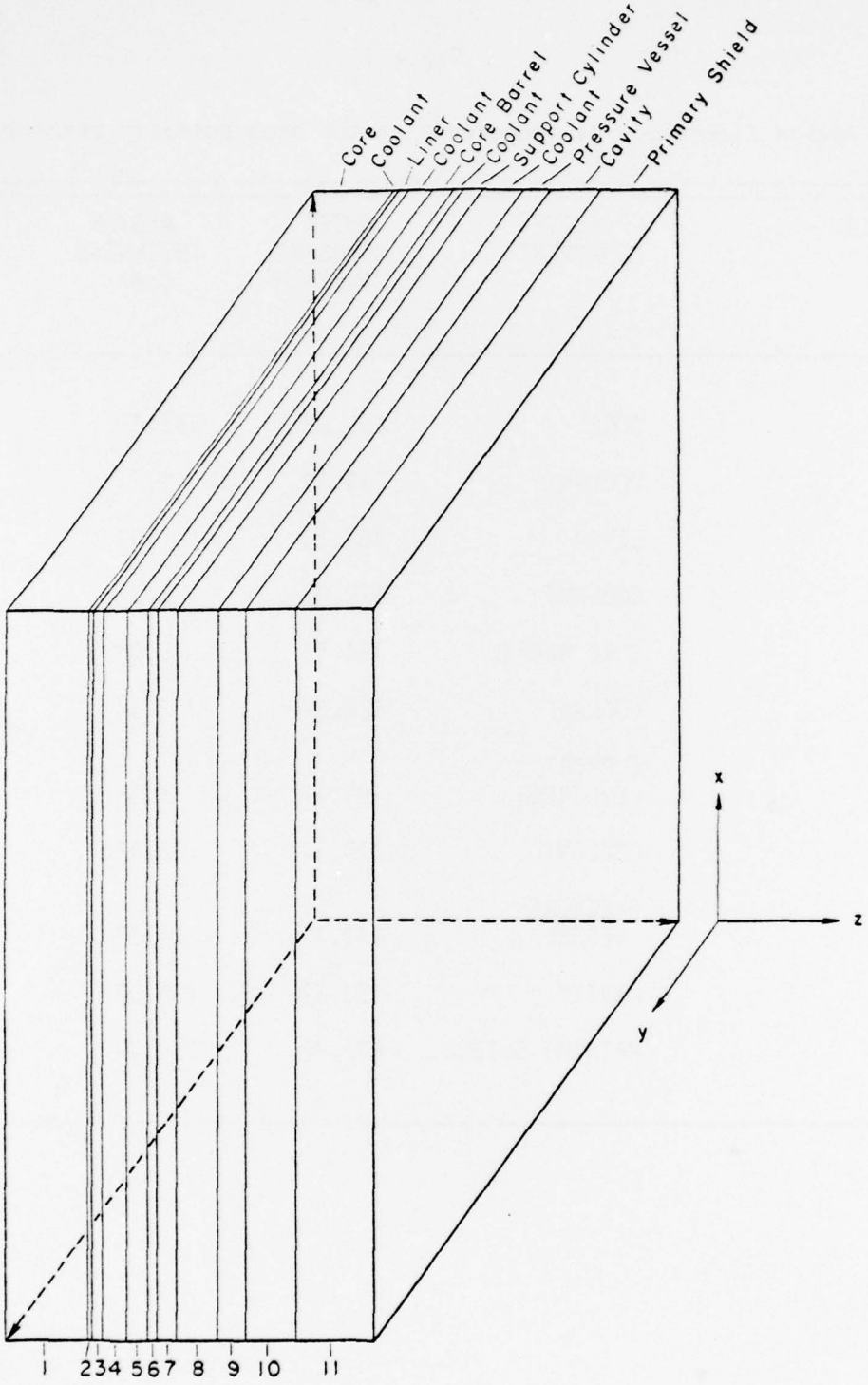

Fig. 1 - Slab reactor geometry

Table 1

Region dimensions of components of the slab geometry reactor

REGION	REACTOR COMPONENT	OUTER BOUNDARY (cm)	REGION THICKNESS (cm)
1	CORE	163.58	163.58
2	COOLANT	163.79	0.21
3	LINER	165.70	1.91
4	COOLANT	179.07	13.37
5	CORE BARREL	184.15	5.08
6	COOLANT	186.69	2.54
7	SUPPORT CYLINDER	191.77	5.08
8	COOLANT	217.17	25.40
9	PRESSURE VESSEL	238.44	21.27
10	CAVITY	350.52	116.08
11	PRIMARY SHIELD	502.92	152.40

Table 2

Material composition of the reactor components

REGION	NAME	MATERIAL	ATOMIC DENSITY atoms/cm^3
1	CORE	HOMOGENEOUS MIXTURE OF	
		HYDROGEN	2.6822E + 22
		OXYGEN	2.7353E + 22
		SILICON	1.4044E + 18
		CHROMIUM	5.3533E + 19
		MANGANESE	1.3968E + 18
		IRON	3.5749E + 19
		NICKEL	1.9742E + 20
		ZIRCONIUM	4.3645E + 21
		U-235	1.9690E + 20
		U-238	6.7739E + 21
		Pu-239	3.4120E + 19
		Pu-240	7.6676E + 18
2	COOLANT	BORATED WATER (600^{o}F, 2250 PSI, 17PPM B)	
		HYDROGEN	4.6220E + 22
		OXYGEN	2.3110E + 22
		BORON-10	1.396E + 17
3	LINER	STAINLESS STEEL (TYPE 304)	
		CARBON	2.3767E + 20
		SILICON	8.8462E + 20
		CHROMIUM	1.7386E + 22
		MANGANESE	1.5156E + 21
		IRON	5.8072E + 22
		NICKEL	8.5091E + 21
4	COOLANT	BORATED WATER (600^{o}F, 2250 PSI, 17PPM B)	
5	CORE BARREL	STAINLESS STEEL (SS304)	
6	COOLANT	BORATED WATER	
7	SUPPORT CYLINDER	STAINLESS STEEL (SS304)	
8	COOLANT	BORATED WATER	

9	PRESSURE VESSEL	STEEL (A533B)		
			CARBON	8.6704E + 20
			ALUMINUM	7.0177E + 19
			SILICON	4.2029E + 20
			CHROMIUM	1.2746E + 20
			MANGANESE	1.1201E + 21
			IRON	8.1974E + 22
			NICKEL	4.8377E + 20
			MOLYBDENUM	2.7137E + 20
10	CAVITY	AIR (150°F, 15PSI)		
			NITROGEN	3.413E + 19
			OXYGEN	9.156E + 18
11	PRIMARY SHIELD	ORDINARY CONCRETE		
			HYDROGEN	8.6089E + 21
			CARBON	1.1423E + 20
			OXYGEN	4.3289E + 22
			SODIUM	9.6396E + 20
			MAGNESIUM	1.2392E + 20
			ALUMINUM	1.7410E + 21
			SILICON	1.6618E + 22
			POTASSIUM	4.6060E + 20
			CALCIUM	1.5028E + 21
			IRON	3.4503E + 20

$$S(Z,E) = 1.823 \times 10^5 \; P(Z) \quad (E) \; n/sec \qquad (1)$$

The proportionality constant was chosen to express the strength function for this reactor in units of neutrons per second. It also includes a correction factor of 1.55 (the product of azimuthal and axial peaking factors) to take into account the fact that the maximum flux occurs out of the mid-core plane since the core and its power distribution are really not slab or cylindrically symmetric.

Because of the symmetry of the core power distribution and the reactor medium, one need not sample the entire volume source, but only the line source distribution along X=Y=0. The thickness of the core slab was taken equal to the core radius; a specular reflection boundary condition at the plane Z=0 was used to more closely correspond to the near cylindrical geometry of the core.

III. BIASING

A. Spatial biasing of the source

Since the core has a thickness of 163.58 cm and we wish to know the flux out to and through the pressure vessel wall which is many mean free paths away, it is necessary to bias the source spatial distribution so that most of the neutrons are selected from near the surface. Otherwise few of the source neutrons selected will get out

Table 3

Core power distribution for slab geometry

INTERVAL MIDPOINT (cm)	INTERVAL WIDTH (cm)	RELATIVE POWER DENSITY (cm^{-1})	SLAB RELATIVE POWER P(z)
8.3333	16.6667	0.94226	15.705
25.000	"	.97196	16.198
41.667	"	.99001	16.500
58.333	"	.97394	16.232
75.000	"	.94643	15.773
91.667	"	.95221	15.870
101.36	2.72727	.96924	2.6434
104.09	"	.96529	2.6326
106.82	"	.95953	2.6169
109.55	"	.95569	2.6064
112.27	"	.96169	2.6234
115.00	"	.97221	2.6542
117.73	"	.98164	2.6772
120.45	"	1.0095	2.7532
123.18	"	1.0672	2.9105
125.91	"	1.1574	3.1565
128.64	"	1.2350	3.3682
130.54	1.08323	1.2581	1.3628
131.62	"	1.2913	1.3988
132.71	"	1.3170	1.4266
133.79	"	1.3370	1.4483
134.87	"	1.3407	1.4523
135.96	"	1.3291	1.4397
137.04	"	1.3091	1.4180
138.12	"	1.2870	1.4049
139.21	"	1.2665	1.3719
140.29	"	1.2495	1.3535
141.37	"	1.2362	1.3391
142.46	"	1.2264	1.3284
143.54	"	1.2190	1.3205
144.62	"	1.2120	1.3129
145.71	"	1.2034	1.3036
146.79	"	1.9111	1.2902
147.87	"	1.1732	1.2708
148.96	"	1.1516	1.2474
150.04	"	1.1303	1.2244
151.12	"	1.1047	1.1966
152.21	1.08323	1.0714	1.1606
153.29	"	1.0304	1.1162

154.37	"	.97903	1.0605
155.46	"	.92429	1.0012
156.54	"	.86173	.9335
157.62	"	.80526	.87228
158.71	"	.74459	.80656
159.79	"	.70086	.75919
160.87	"	.66114	.71617
161.96	"	.62466	.67665
163.04	"	.58864	.63763

Table 4

Source neutron energy spectrum

NEUTRON ENERGY GROUP NO. g	UPPER EDGE GROUP ENERGY (MeV)	NORMALIZED RELATIVE PROBABILITY (g)
1	14.92	0.16000E-03
2	12.20	0.90000E-03
3	10.00	0.35000E-02
4	8.180	0.13970E-01
5	6.360	0.34730E-01
6	4.960	0.35220E-01
7	4.060	0.10778E+00
8	3.010	0.89410E-01
9	2.460	0.23300E-01
10	2.350	0.12091E+00
11	1.830	0.21913E+00
12	1.110	0.19937E+00
13	.5500	0.13605E+00
14	.1110	0.15570E-01

and an inordinate number of histories will be needed to obtain a reasonable variance in the flux at the pressure vessel. The original neutron spatial distribution P(Z) was biased therefore by the factor $\exp((Z_o-Z)/\lambda)$, where Z_o is the core radius and λ is an average neutron mean free path in the core, so that the frequency of selection of the neutron starting position in the core was roughly proportional to the probability of the neutron escaping from the core. The weight of the selected neutron is then modified so that for each interval the product of starting weight, W_i, and the probability of picking a neutron from that interval is invariant. That is, if Z_i is the midpoint of the ith interval

$$W_i P(Z_i) = C W_i' P'(Z_i) = C W_s' P(Z_i) \exp -(Z_o - Z_i)/\lambda] \quad (2)$$

$$\text{where } C = \Sigma P(Z_i) \exp (Z_i - Z_o)/\lambda]^{-1}. \quad (3)$$

Therefore, the modified weight of the neutron, W_i', is

$$W_i' = (W_i/C) \exp[+(Z_o-Z_i)/\lambda] \quad (4)$$

In the actual calculation we took λ = 7 cm. The MORSE subroutine SOURCE was written to incorporate this biasing feature and is listed in Appendix I.

B. Source energy biasing

The source neutron energy distribution function $\chi(E)$ as shown in Table 4 peaks in the 1-2 MeV range and the neutrons in the 10-15 MeV range are 100-1000 times less probable. It was necessary to employ energy biasing in the source, since we are interested in the fast neutron flux out to the pressure vessel wall and contributions to the flux will be greater for those neutrons starting out with the higher energies. The lower energy neutrons will undergo so many collisions that their energy will be well below 1 MeV before they reach the wall and their contributions to the fast flux will be negligible. An energy biasing function $B(E)$ was chosen such that the frequency of selection of neutron energies was approximately uniform over the energy region sampled. That is all energy groups are equally likely to be chosen. In this case the modified energy distribution, $\chi'(E_i)$ is obtained by multiplying the corresponding $\chi(E_i)$ by the biasing factor $b/B(E_i)$, where $B(E)$ is tabulated in Table 5, and the constant, b, is such that the new distribution χ' is normalized.

C. Path-length stretching

Another form of biasing that we employed in the calculation of the neutron flux is known as path-length stretching. Instead of using the physical mean free path, λ, between collisions, the mean

Table 5

Energy viasing factors for source neutrons and at collision sites

GROUP No.	UPPER EDGE ENERGY GROUP MeV	SOURCE NEUTRON ENERGY BIASING FACTOR B(E)	COLLISION ENERGY BIASING FACTOR
1	14.92	0.0495	1.28 E+02
2	12.20	0.1052	6.40 E+01
3	10.00	0.1702	3.20 E+01
4	8.180	0.2481	1.60 E+01
5	6.360	0.3125	8.00 E+00
6	4.960	0.3780	4.00 E+00
7	4.060	0.4447	2.00 E+00
8	3.010	0.5001	1.75 E+00
9	2.460	0.5722	1.50 E+00
10	2.350	0.6471	1.25 E+00
11	1.830	0.7827	1.00 E+00
12	1.110	0.9061	7.50 E-01
13	0.550	0.9904	6.00 E-02
14	0.110	1.000	3.00 E-02

free path in a direction of interest can be effectively increased by a factor denoted "BIAS" in MORSE, so that, e.g., the neutron travels further in the direction of the pressure vessel before encountering a collision.

The factor BIAS is defined in terms of two other parameters,

$$BIAS = \frac{1}{1-(PATH)(DIREC)} \tag{5}$$

where PATH is a measure of how much stretching is to be applied and lies between 0 and 1 and DIREC is taken as the cosine of the angle between the flight direction and the direction in which one wants to encourage the neutrons to go. This technique will improve counting statistics in regions in the direction of the pressure vessel at the expense of a loss in statistics in the local region where the biasing is applied. When properly applied this tradeoff is beneficial. The results tabulated herein were calculated with path stretching parameters (PATH) shown in Table 6.

D. Energy biasing at collision sites

As a neutron enters a collision its outgoing energy and direction after collision are determined by first sampling the group to group transfer matrices to obtain the new energy and then the

Table 6

Values of the path length stretching parameter PATH

REGION	REACTOR COMPONENT	VALUE OF "PATH"
1	Core	0.75
2	Coolant	0.0
3	Liner	0.0
4	Coolant	0.5
5	Core Barrel	0.0
6	Coolant	0.0
7	Support Cylinder	0.0
8	Coolant	0.5
9	Pressure Vessel	0.5
10	Cavity	0.0
11	Primary Shield	0.6

angular distribution that is kinematically consistent with this neutron energy. Low energy neutrons near the core are less likely to contribute to the fast flux at the vessel wall, and so one would like to bias the outgoing energy distribution toward higher energies.

In MORSE one can also bias the sampling of the group to group energy transfer probability at collision sites so that by employing these multiplicative bias factors, on the average higher energy neutrons are selected at each collision. The set of bias factors used in this calculation is shown in Table 7.

The comparison in slab and cylindrical geometry between MORSE and ANISN in this report does not include collision biasing.

E. Russian roulette and splitting

There are two other options available in MORSE for decreasing variance and increasing efficiency. When the weight of a neutron becomes so small that it is inefficient to follow its history, one can "play" Russian Roulette. With a certain probability, the particle is either "killed" or its weight is increased so that it pays to follow it again. When the weight of a particle, on the other hand, is too large and its contribution, or lack of it, may cause a large fluctuation in the final result, one may split that particle into a number of particles each having a smaller weight. We found neither of

Table 7

Comparison of fast neutron flux using MORSE and ANISN in slab geometry

RADIUS (cm)	ANISN (Flux) E > 1.0 MeV	MORSE(SLAB) (Flux) E > 1.0 MeV	Standard Deviation %	MORSE/ANISN
163.58	4.60E +13	4.58E +13	+2	1.00
163.79	4.42E +13	4.39E +13	+2	0.99
165.70	2.64E +13	2.62E +13	+2	0.99
169.04	1.35E +13	1.43E +13	+3	1.06
172.39	8.27E +12	8.61E +12	+3	1.04
175.72	5.49E +12	5.70E +12	+4	1.04
179.07	4.29E +12	4.52E +12	+4	1.05
181.61	3.25E +12	3.12E +12	+4	0.96
184.15	1.98E +12	1.84E +12	+4	0.93
186.69	1.43E +12	1.45E +12	+5	1.01
191.77	5.93E +11	6.21E +11	+13	1.05
200.24	1.48E +11	1.64E +11	+11	1.11
208.71	5.36E +10	5.98E +10	+34	1.12
217.17	2.80E +10	2.03E +10	+15	0.73
222.49	1.68E +10	1.09E +10	+20	0.65
227.81	8.36E +9	1.09E +10	+42	1.13
233.12	4.00E +9	3.97E +9	+25	.99
238.44	1.73E +9	1.66E +9	+38	0.96

these options to be very useful in our calculation of fast flux and so did not use them.

IV. NEUTRON FLUX ESTIMATORS

A. Boundary crossing or surface crossing estimators (BDRYX)

This method is particularly useful for estimating the flux in a one dimensional geometry. We can obtain the contribution to the average flux on each boundary or surface crossed by the ith neutron by scoring the weight (when crossing) of that neutron, W_i, divided by the absolute value of the cosine of the angle between the neutron track and the normal to the surface:

$$\Phi(Z) = \sum_i \frac{W_i}{|\cos \theta_i|} \tag{6}$$

Because of the symmetry of the medium and the source distribution, the flux is uniform on any symmetry surface. Hence the flux at any <u>point</u> on that surface is equal to the average flux over the surface.

A difficulty with the boundary crossing estimator is that the variance associated with it is unbounded. It is clear that for grazing angles $\theta \sim \pi/2$, $1/\cos\theta$ is very large, making a very large contribution to the sum and the variance. To avoid these large fluctuations, we limit the magnitude of $\cos\theta$, by setting $\cos\theta$ to 0.005 for all angles such that $\cos\theta \leq .01$.

This estimator is implemented in the subroutine BDRYX and is listed in Appendix II.

The subroutine BDRYX is called whenever a neutron track crosses the boundary of a geometry medium. Even if the problem has only one real medium, different geometry media can be artificially defined so that scoring surfaces can be established wherever they are desired. These geometry media are defined in the input to MORSE and obtained from subroutine GTMED, which is listed in Appendix III.

B. Next-event uncollided estimator (UNC)

In the surface crossing estimator previously discussed neutrons had to actually cross the surface or boundary in order to be scored. We can also use a so called expected value estimator which relates the emergent particle density at a collision site to the flux $\Phi(Z)$. Thus a contribution to the flux is made at every collision. The flux as calculated by this estimator is given by[4]

$$\Phi(Z) = \sum_i \frac{W_i \exp(-\Sigma_t R_i)}{|\cos\theta_i|} + U(Z) \qquad (7)$$

where W_i is the statistical weight after collision, $\Sigma_t(E_i)$ is the macroscopic total neutron scattering cross section for the emergent particle of energy E_i, R_i is the distance, in the direction of the velocity of the emergent particle, between the ith collision site and the plane. This flux estimate is implemented in

subroutine RELCOL. Because this subroutine is only called at collision sites, a separate analytic contribution, U(Z), from the source site must be made--the uncollided flux contribution.

C. Tracklength per unit volume estimator (TLPUV)

The neutron weighted total path length within some control volume, divided by that volume is the average flux throughout the volume:[4]

$$\Phi = \frac{1}{\Delta V} \sum_i W_i L_i \tag{8}$$

A large control volume can be chosen to improve statistics, but a small control volume will give a more accurate value of the flux at a point. We have also included this estimator for comparison with the others. In MORSE the estimate can be obtained from subroutine ENDRUN. However no variance on the estimate is given there.

If the neutron suffers many collisions within the control volume, this method becomes rather inefficient and estimators based on the density of collisions should be considered.

D. Collision density concept of flux (COLDEN)

If within some control volume, ΔV, the weighted total number of Monte Carlo collisions of neutrons in energy group g_i is given by $n(g_i)$, then the average flux in the control volume is given by[4]

$$\Phi = \sum_i \frac{n(g_i)}{\Sigma_t(g_i)\Delta V}, \tag{9}$$

where Σ_t is the total macroscopic scattering cross section. This method works well when there are many scattering collisions in the control volume. Again, for comparison purposes, a flux estimate based on this model is also given. It also can be obtained from the subroutine ENDRUN.

V. VARIANCE REDUCTION VIA PATHLENGHT STRETCHING AND ENERGY BIASING AT COLLISION SITES (Collision Biasing)

In the simple slab geometry we have computed the fast flux as a function of radial distance from the reactor core for 900 neutron histories to determine how path length stretching and energy biasing at collisions affect the variance for the boundary crossing and next-event uncollided estimators. These were test cases performed to look for qualitative trends and clearly were not made to reduce the variance to the lowest possible value.

The calculated fractional standard deviation for the UNC estimator is plotted versus radial distance from the core in Fig. 2 for the path length stretching parameters shown in Table 6. On the average, there is a definite variance reduction for distances beyond 180 cm for the path length stretched calculations. For distances less than 180 cm there are no observable differences .

A similar comparison is made for the UNC estimator with and without collision biasing. The collision biasing factors were optimized empirically and are tabulated in Table 6. A plot of these results is shown in Fig. 3. Again there is a significant variance reduction for the fast flux beyond distances of 190 cm. For distances less than 190 cm we were able to see no significant difference in the variance.

In Fig. 4 we have plotted the results when both collision biasing and path length stretching were used and when neither was used. Again, beyond 190 cm, there is a significant reduction in variance for the biased case. We conclude that utilization of collision biasing and path length stretching will yield more accurate flux values near the pressure vessel wall for a given number of neutron histories.

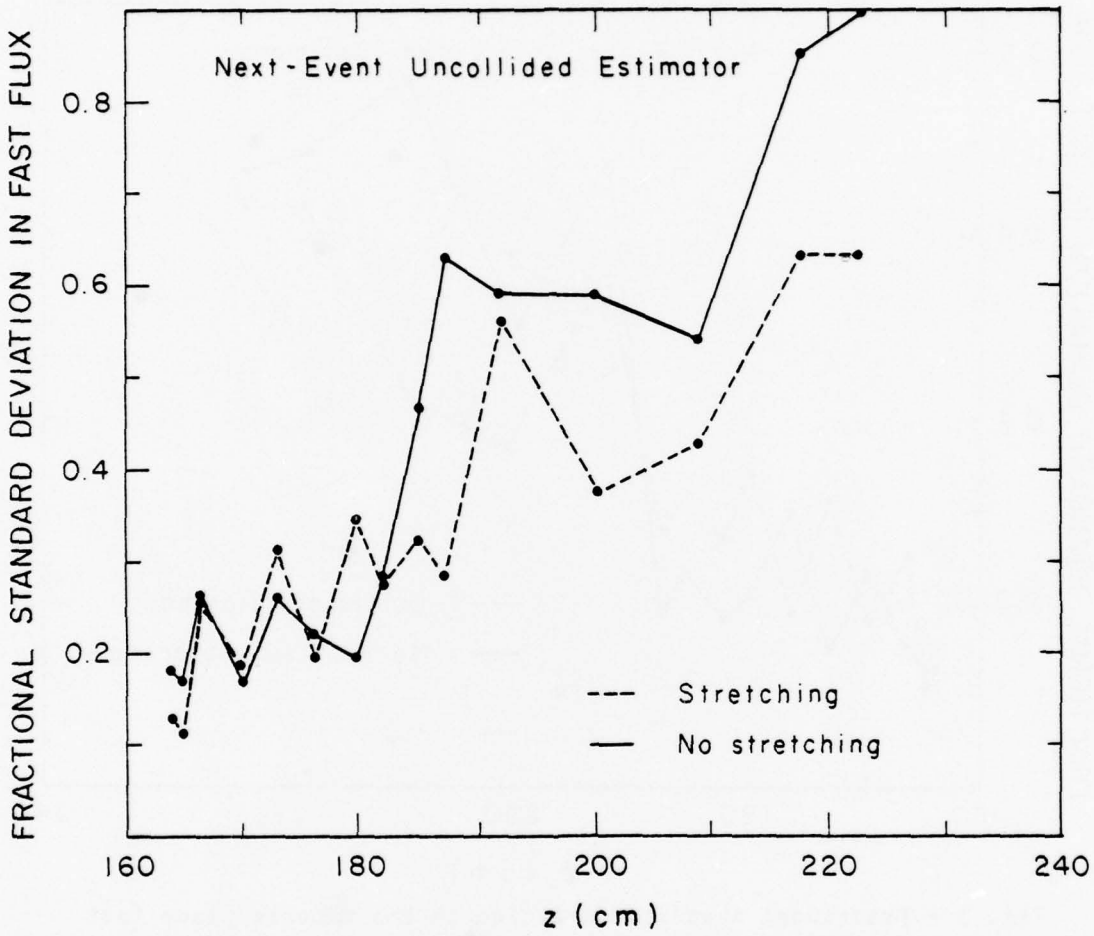

Fig. 2 - Fractional standard deviation in the midcore plane fast flux with and without stretching

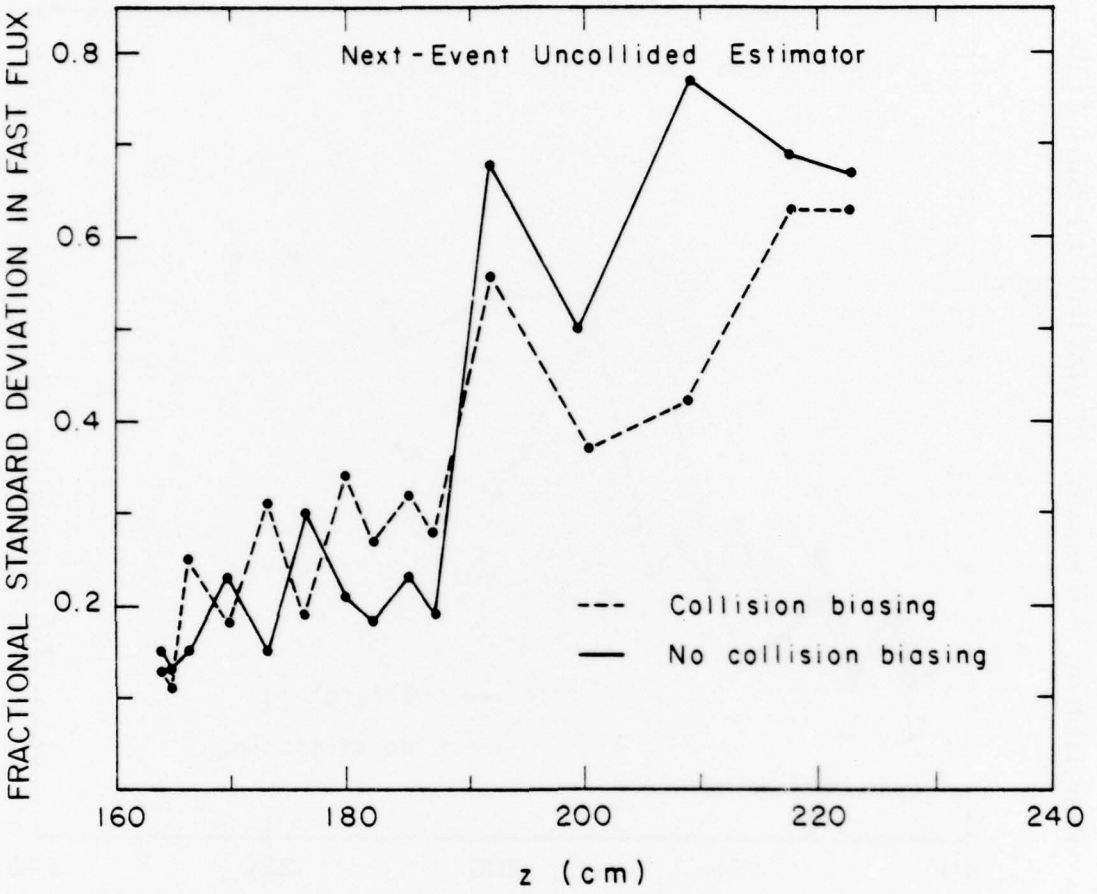

Fig. 3 - Fractional standard deviation in the midcore plane fast flux for UNC estimator with and without collision biasing

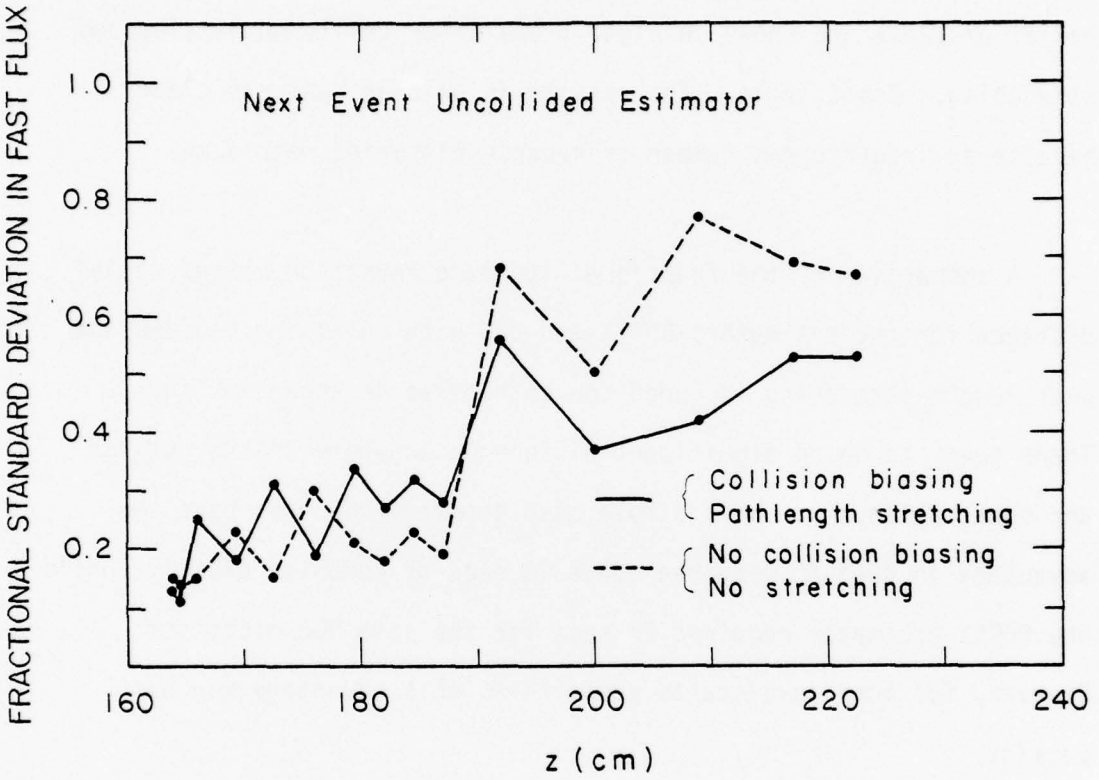

Fig. 4 - Fractional standard deviation in the midcore plane fast flux for UNC estimator with both collision biasing and stretching and without either

VI. COMPARISON OF BDRYX WITH UNC

We have performed a similar analysis for the boundary crossing estimator (BDRYX). The plots of fractional standard deviation versus radial distance are shown in Figs. 5 and 6 for collision biasing and stretching, respectively. The results in neither case are clear because an insufficient number of neutron histories was taken.

A comparison of the fractional standard deviation versus radial distance for the estimators BDRYX and UNC with collision biasing and path length stretching included for both cases is shown in Fig. 7. There seems to be no significant difference anywhere in the outside the core region. For this simple slab geometry UNC does have the advantage in that it required about 13 secs of computer CPU time while the BDRYX estimator required 21 secs for the same 900 histories. However, for more complicated geometries, this advantage may not persist.

VII. COMPARISON OF THE MONTE CARLO SLAB MODEL FAST FLUX RESULTS WITH ANISN

The final slab geometry Monte Carlo calculations were performed using 200,000 neutron histories and the boundary crossing estimator. At the same time the fast flux was also estimated by track length per unit volume and collision density estimators. These last two

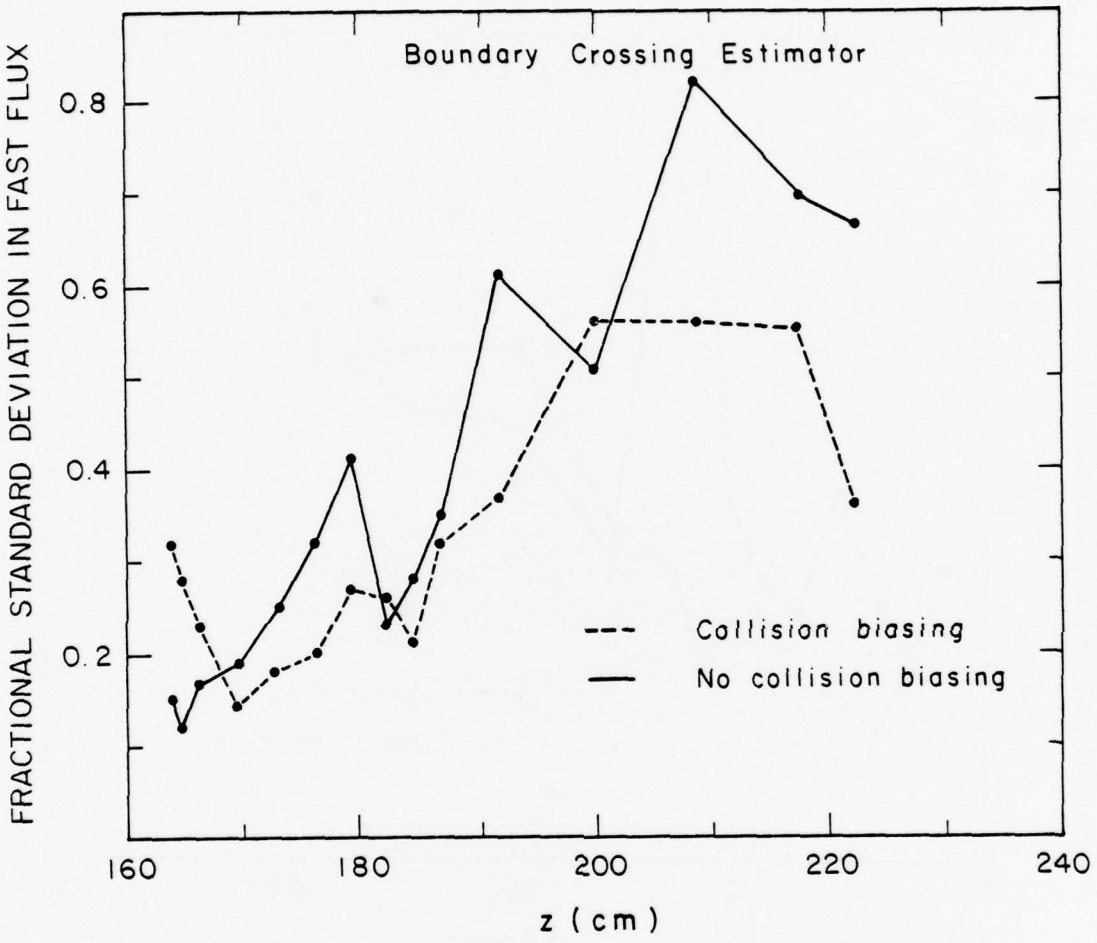

Fig. 5 - Fractional standard deviation in the midcore plane fast flux for BDRYX estimator with collision biasing

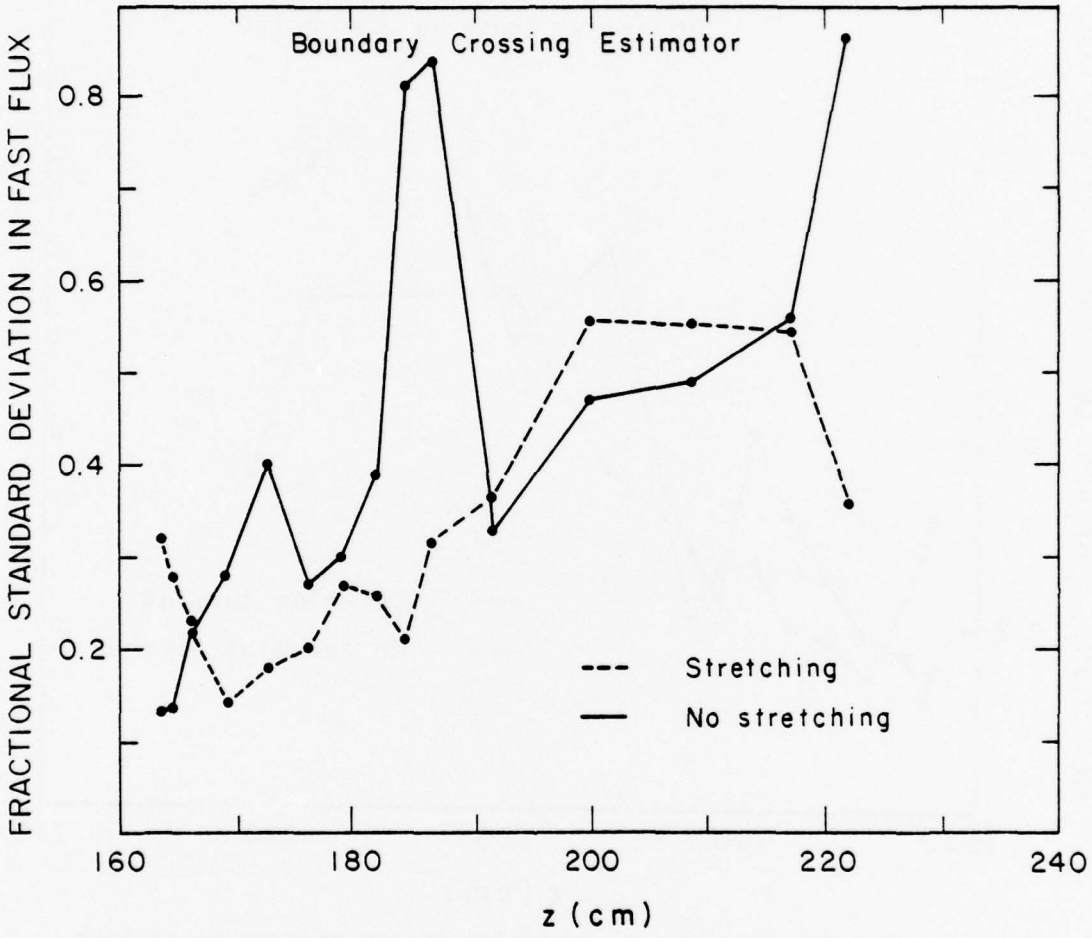

Fig. 6 - Fractional standard deviation in the midcore plane fast flux for BDRYX estimator with stretching

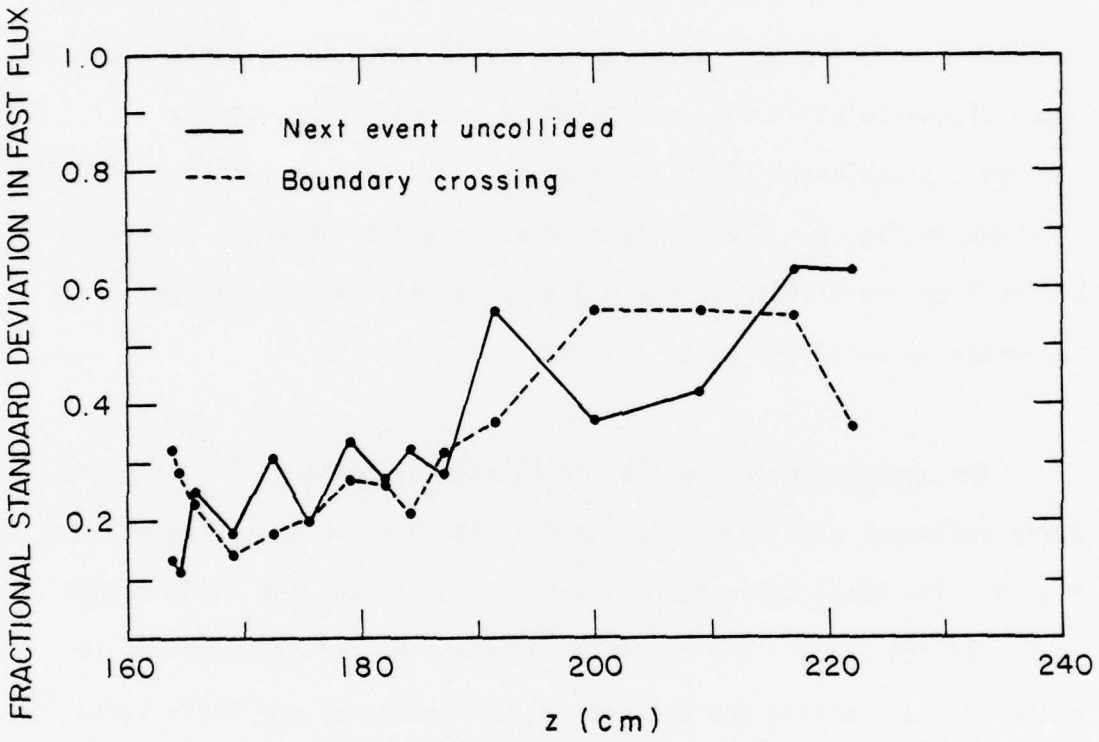

Fig. 7 - Fractional standard deviation in the midcore plane fast flux for BDRYX and UNC with collision biasing and stretching

estimators were useful as a check on BDRYX to be sure no gross errors were built into BDRYX. Since these two estimators averaged flux over a volume between two regions instead of giving the flux at a boundary of a region, an exact comparison to BDRYX cannot be expected. Source energy and spatial biasing were used. The path length stretching parameters were empirically optimized and the final set is tabulated in Table 1. No energy biasing at the collision sites was employed. A graph of the relative flux estimated by the collision density (COLDEN), tracklength (TLPUV) and boundary crossing estimators (BDRYX) is shown in Fig. 8. The collision density and tracklength estimates of the flux are plotted at the midpoint between two boundaries. The agreement is excellent up to 190 cm.

The comparison of the flux calculated by Monte Carlo using the BDRYX estimator with that calculated by ANISN is shown in Table 7 and Fig. 9. The Monte Carlo results are the points and the ANISN result is the smooth curve. The agreement between the two calculations is quite good and within the statistical variations of the Monte Carlo results. For distances less than 200 cm the statistical errors were less than 3%. In the vicinity of the pressure vessel wall the fractional standard deviation is more like 10-20%. For a more precise comparison in this region further biasing techniques to reduce the variance would be helpful. One can say, however, that the agreement between ANISN and Monte Carlo near the pressure vessel wall is within 20%.

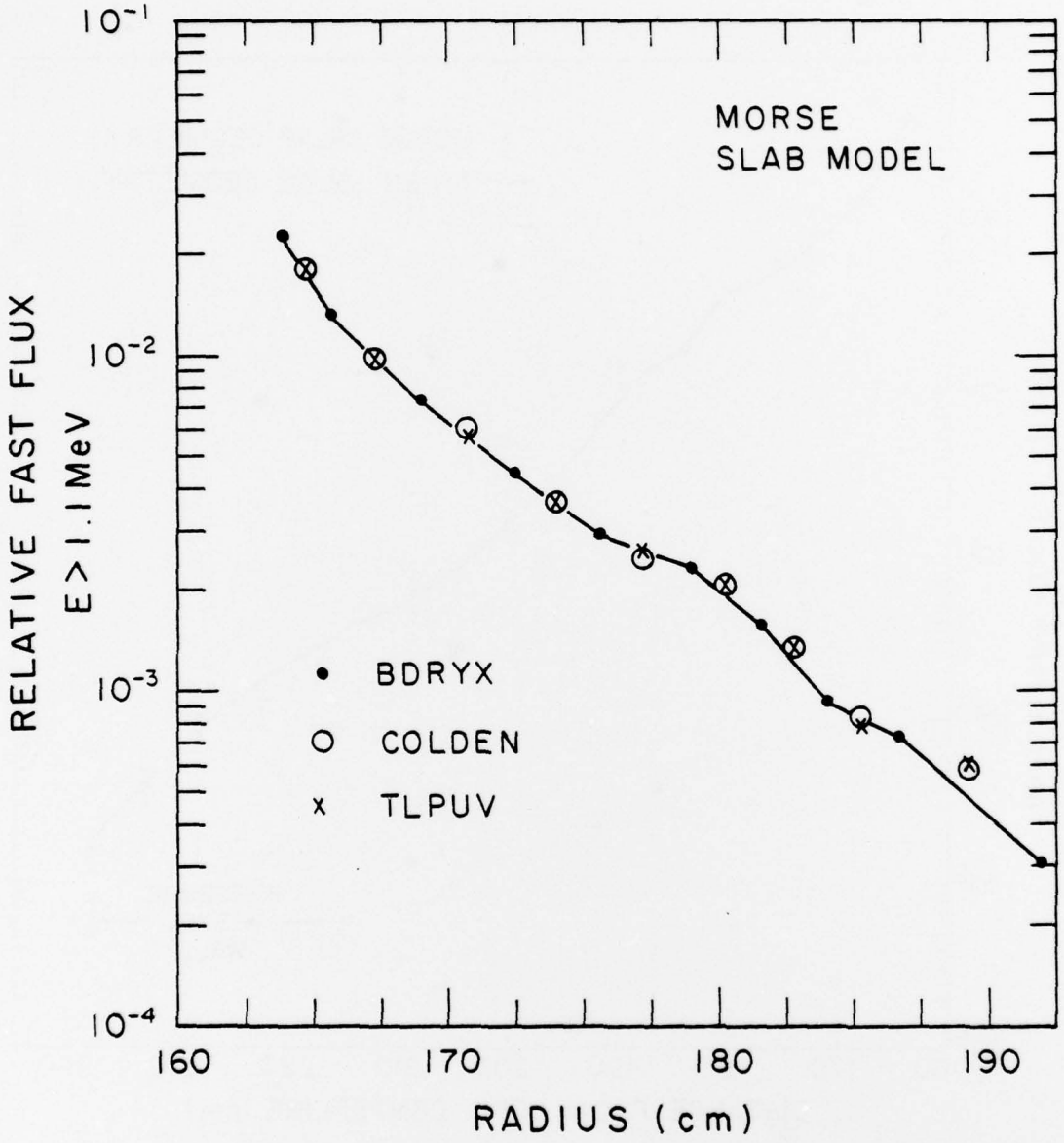

Fig. 8 - Comparison of fast flux as a function of radial distance estimated by BDRYX, TLPUV, and COLDEN

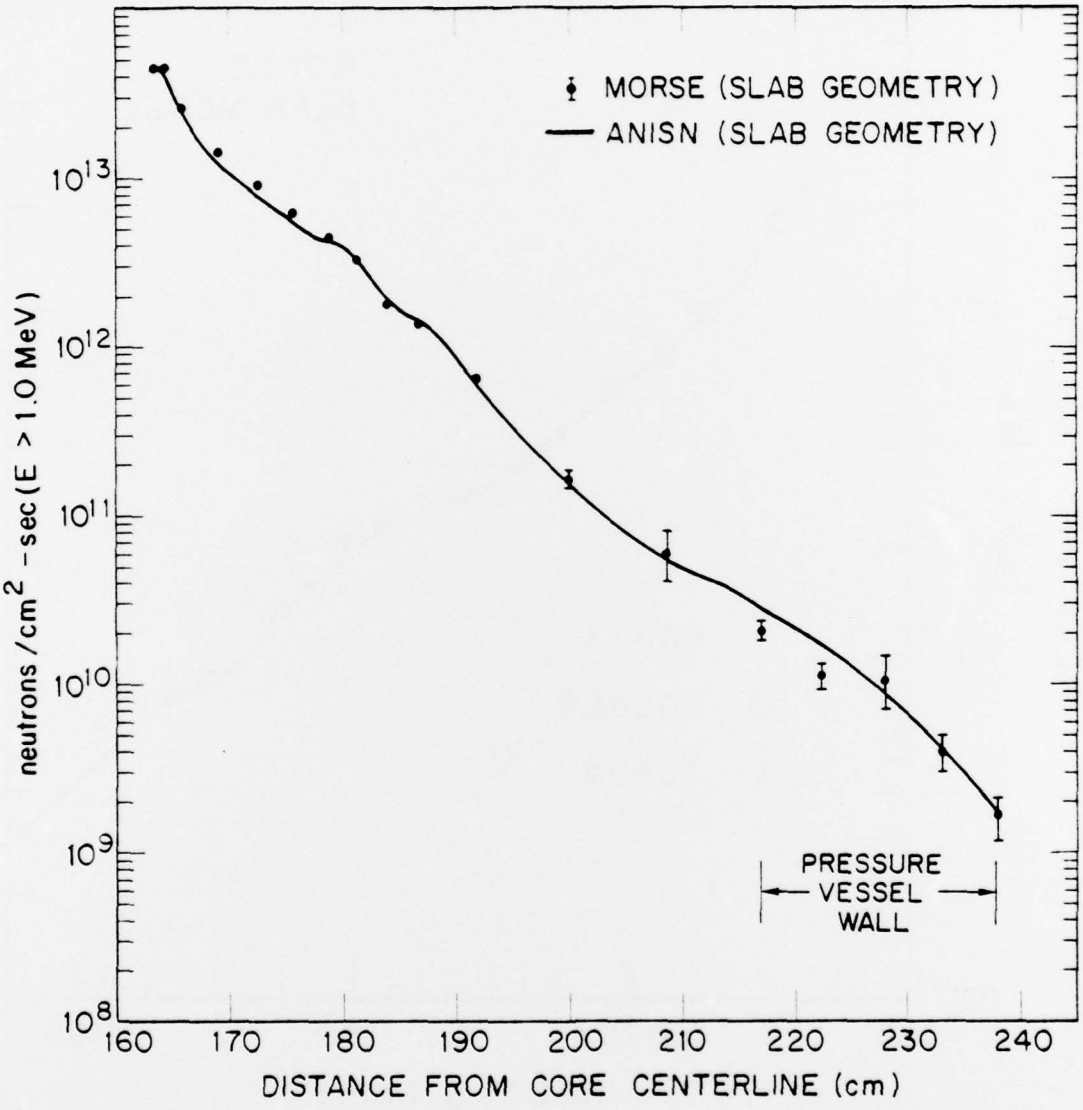

Fig. 9 - Fast flux calculated by MORSE and ANISN using slab models

A comparison of the neutron energy spectra at the inside of the pressure vessel wall is shown in Fig. 10. Again, on the average, the agreement between ANISN and Monte Carlo is within the statistical uncertainty of the Monte Carlo results.

VIII. MORSE MONTE CARLO CALCULATION IN THE CYLINDRICAL MODEL

A. Cylindrical model geometry and neutron source parameters.

Since the major reactor components are more nearly cylinders than slabs, a better approximation would be to calculate the neutron flux using cylindrical shells instead of slabs. In the cylindrical geometry Monte Carlo calculation also the height of each cylinder was taken to be 20,000 cm and the outer radius of each annulus is the same as in Table 1. Since the reactor core and shielding components are cylindrically symmetric, the flux will be uniform on any cylindrical surface. That is, the flux averaged over the surface is the flux at any point on the surface. Again we may replace the volume source with a line source and use MORSE to calculate the average flux on cylinders of radius R.

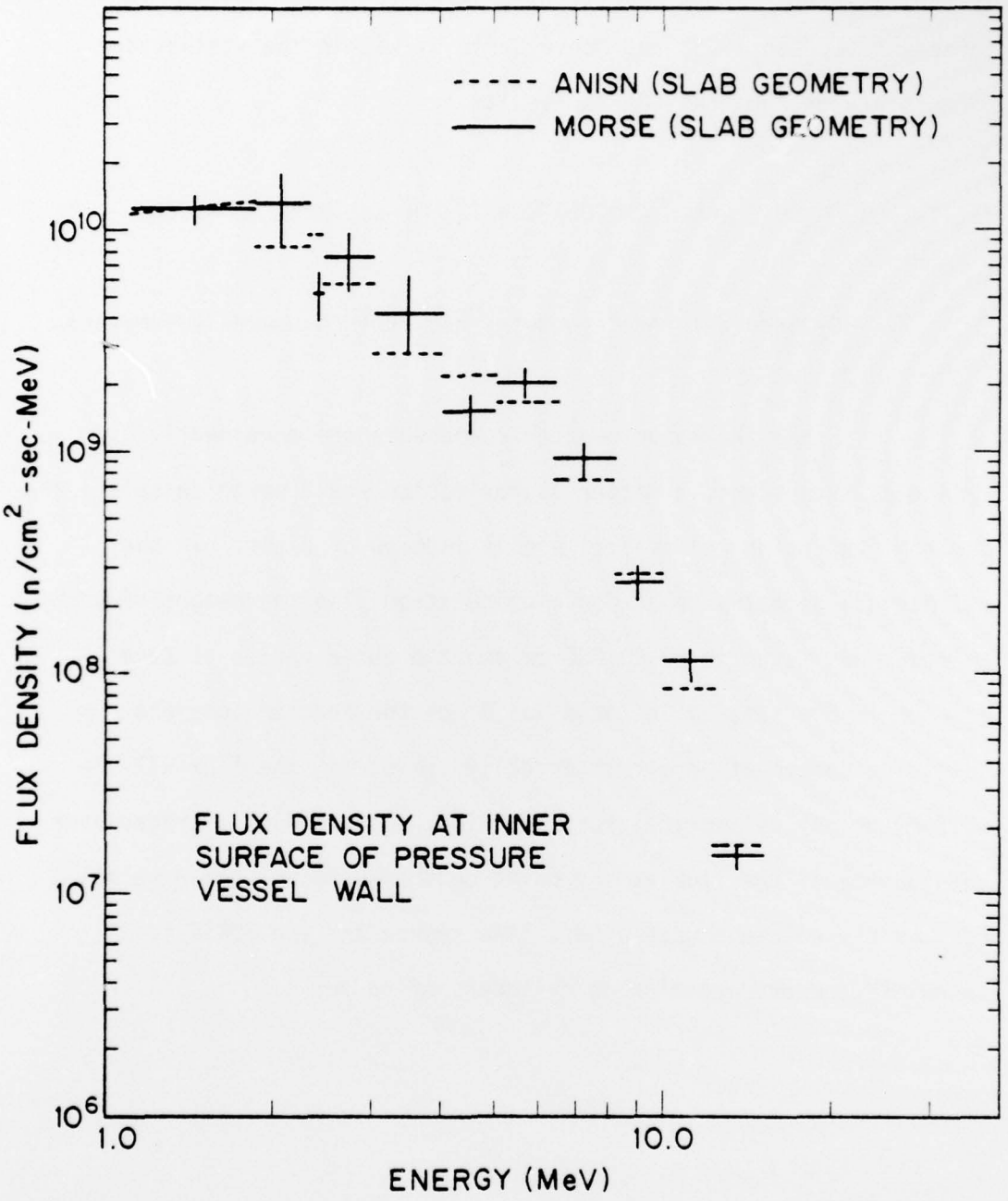

Fig. 10 - Neutron energy spectra at the inside of the pressure vessel wall calculated by MORSE and ANISN using slab models

For the cylindrical calculation we used the same power density as in the slab case. Since the volume of an annulus increases with radius, however, the distribution of relative power for the two cases are different.

The flux estimator used in the cylindrical model was the boundary crossing estimator, suitably modified for cylindrical symmetry. The boundary crossing estimator in the cylindrical case is given by

$$\Phi(R) = \sum_i \frac{R_c}{2R} \frac{W_i}{|\cos\theta_i|} \quad (10)$$

where R_c is the core radius.

The MORSE Monte Carlo results in cylindrical geometry are shown compared to ANISN results in slab geometry in Fig. 11. Within 185 cm from the core center there is little difference outside statistics between the calculations. However, beyond 185 cm the MORSE cylindrical results average are about 30% lower than ANISN. As far as the radiation safety aspects are concerned ANISN is somewhat conservative in predicting a higher value of the neutron flux in the slab model. ANISN calculations in cylindrical geometry were not available.

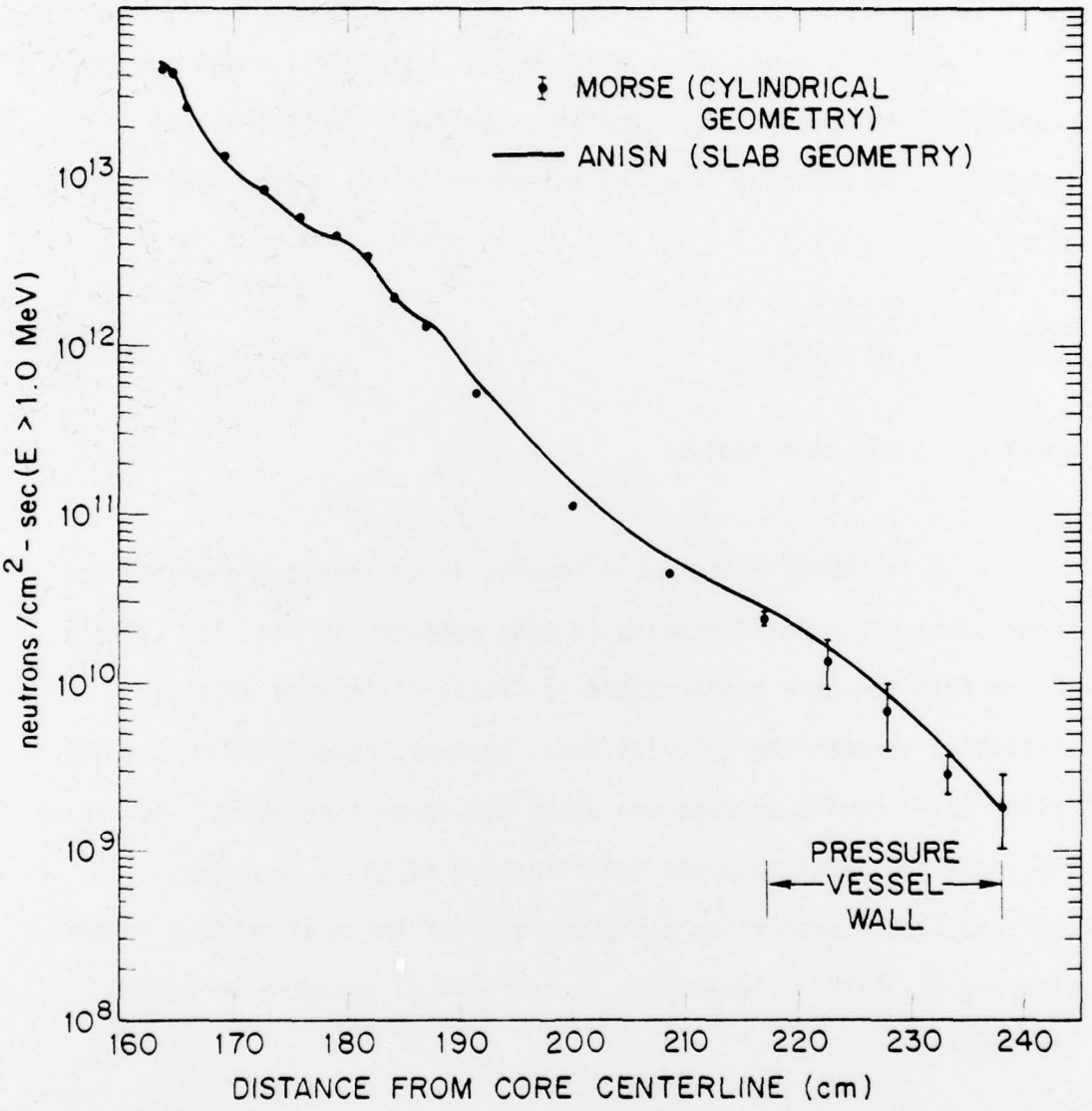

Fig. 11 - Fast flux calculated by MORSE using a cylindrical model and ANISN using a slab model

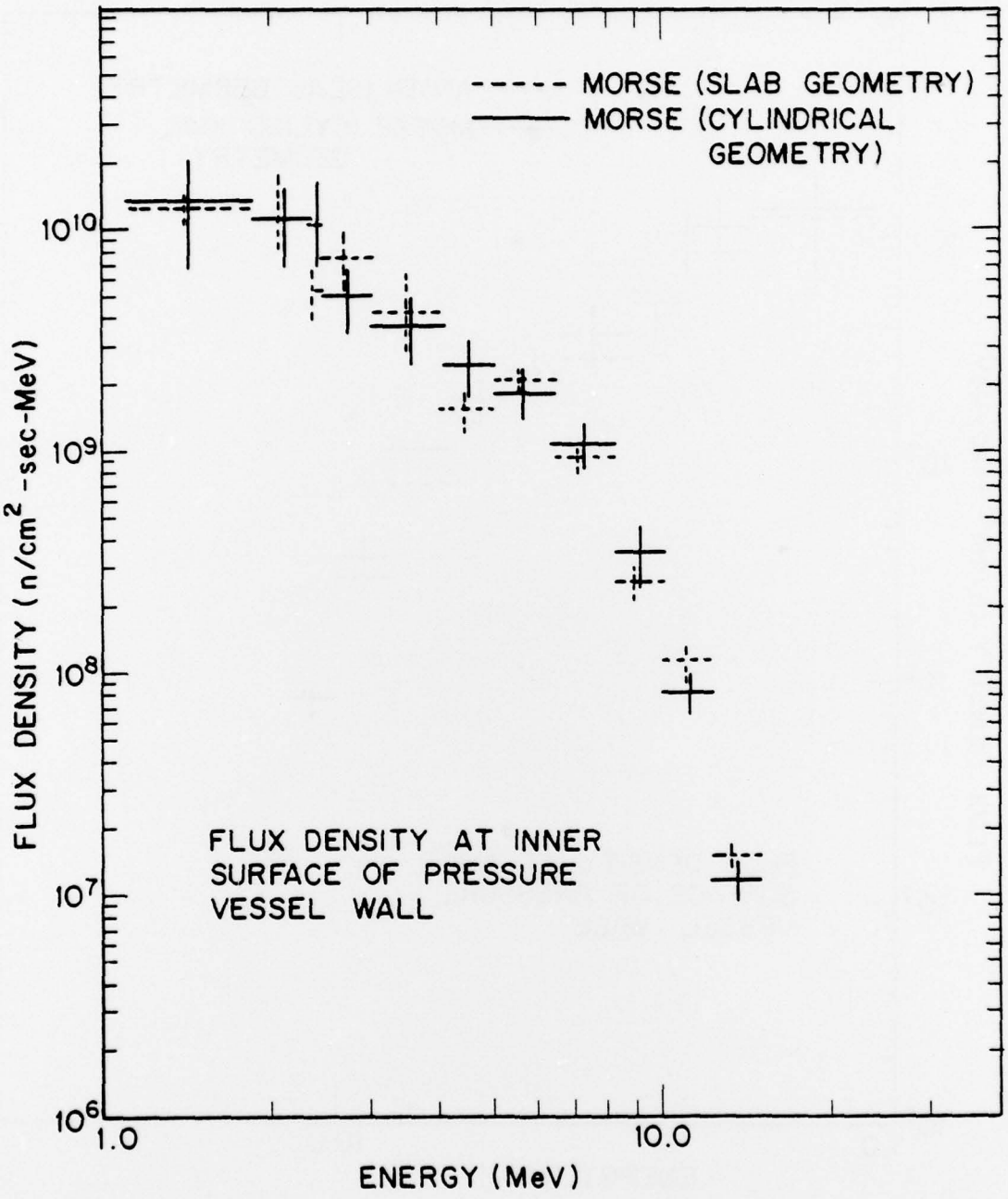

Fig. 12 - Neutron energy spectra calculated by MORSE using a cylindrical model and ANISN using a slab model

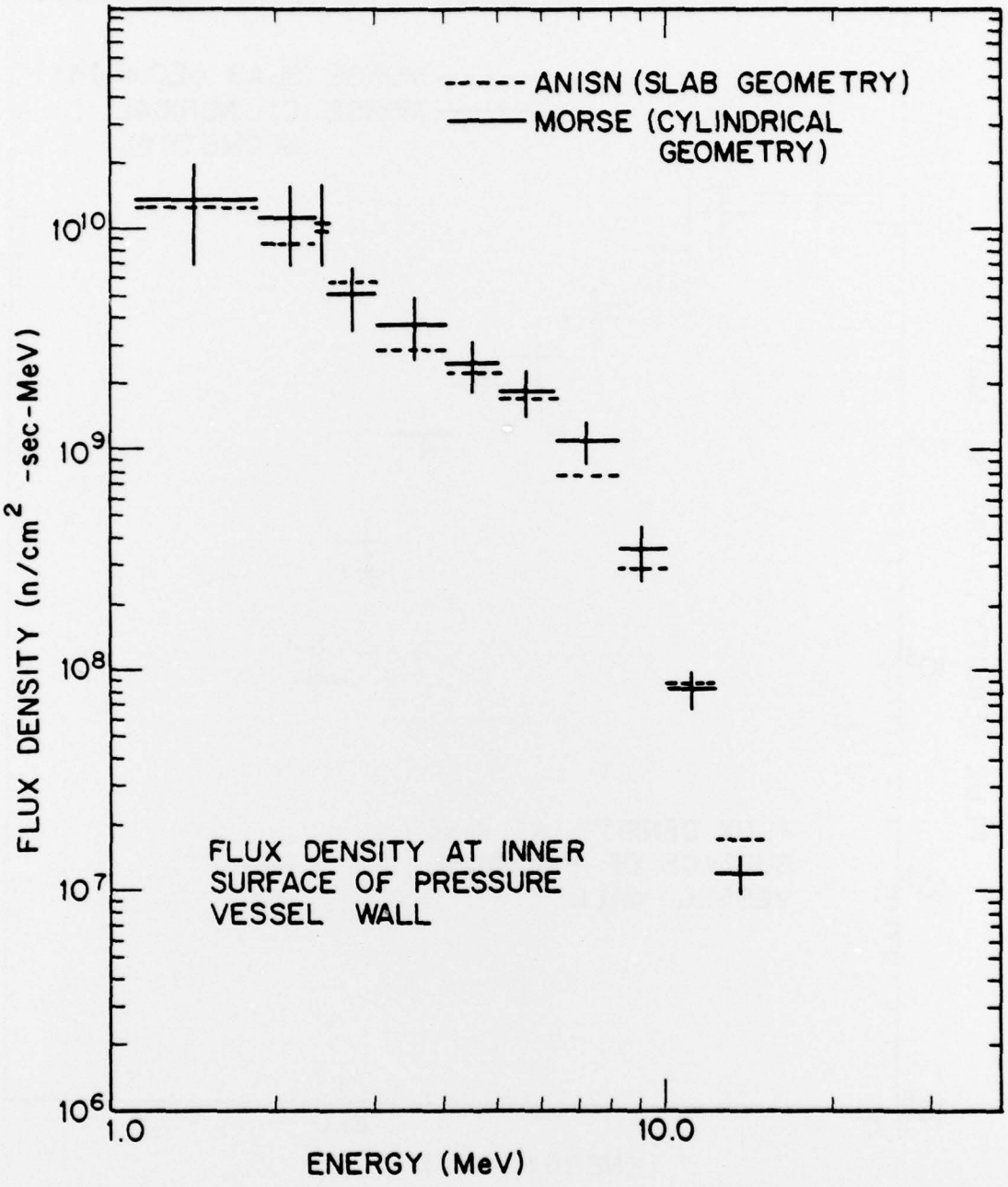

Fig. 13 - Comparison of neutron energy spectra calculated by MORSE using cylindrical and slab models

A comparison of the neutron energy spectra at the inner surface of the pressure vessel wall for ANISN calculated in the slab model and MORSE calculated in the cylindrical model is shown in Fig. 12. Comparison for MORSE in the slab and cylindrical models is made in Fig. 13. In both comparisons no difference in neutron spectra are found at least within the statistical uncertainties of the MORSE calculations.

IX. CONCLUSIONS

The fast neutron flux in the reactor core midplane calculated in slab geometry with the codes MORSE and ANISN were in agreement to within the statistical error of the MORSE calculation. The neutron energy spectra at the inner surface of the pressure vessel wall were also in agreement in this situation. MORSE results in cylindrical geometry show the effect of the 1/r dependence of the flux outside the core; the normalized neutron spectrum at the pressure vessel agreed within statistical error with that calculated in slab geometry.

References

1. M.B. Emmett, RSIC Computer Code Collection, MORSE-CG, CCC-203, Oak Ridge National Laboratory, 1975.

2. H.S. Palme, G.S. Carter, and C.L. Whitmarsh. Babcock & Wilcox Topical Report BAW-10100A, 1975.

3. W.W. Engle, Jr., RSIC Computer Code Collection, CCC-254, Oak Ridge National Laboratory, 1973.

4. J. Spanier and E.M. Gelbard, Monte Carlo Principles and Neutron Transport Problems, Addison-Wesley, 1969.

5. RSIC Data Library Collection, DLC-23B, Oak Ridge National Laboratory, 1975.

6. W.R. Cadwell, et al., The PDQ-5 and PDQ-6 Programs for the Solution of the Two-dimensional Neutron Diffusion-Depletion Problems, WAPD-TM-477, Westinghouse, January 1965.

7. R.J. Breen, O.J. Marlow, and C.J. Pheifer, HARMONY: System for Nuclear Reactor Depletion Computation, WAPD-TM-478, Westinghouse, January 1965.

Appendix I

```
      SUBROUTINE SOURCE (IG,U,V,W,X,Y,Z,WATE,MED,AG,ISOUR,ITSTR,
     1NGPQT3,DDF,ISBIAS,NMTG)
      DIMENSION POW(48),PSPOW(48),RAD(48)
      COMMON WTS(1)
      DATA INIT/0/
      IF(INIT.EQ.1) GO TO 100
      READ (5,63) MRVISO,BTHETA,BF
      READ(5,63) IZBIAS,EMFP,RCORE
      WRITE(6,64) MRVISO,BTHETA,BF
64    FORMAT(10X,"MRVISO=",I5,10X,"BTHETA=",E10.5,10X,"BF=",E10.5)
      WRITE(6,65) IZBIAS,EMFP,RCORE
65    FORMAT(10X,"IZBIAS=",I5,10X,"EMFP=",E10.5,10X,"RCORE=",E10.5)
      IF(IZBIAS.EQ.1) SIGT=1./EMFP
      IF(IZBIAS.NE.1) SIGT=0.0
63    FORMAT (I5,5X,4E10.5)
      CTHETA=COS(BTHETA*6.28/360.)
      FREQ=1./(1.+BF)
      READ(5,10) (RAD(I),I=1,48)
      READ(5,10) (POW(I),I=1,48)
10    FORMAT(5(E11.5,4X))
C     CONSTRUCT SPATIAL GROUP CDF
      PSPOW(1)=POW(1)
      DO 12 I=2,48
12    PSPOW(I)=POW(I)+PSPOW(I-1)
      PSMAX=PSPOW(48)
      PSPOW(1)=POW(1)*EXP(-(RCORE-RAD(1))*SIGT)
      DO 5 I=2,48
5     PSPOW(I)=POW(I)*EXP(-(RCORE-RAD(I))*SIGT)+PSPOW(I-1)
      EPSMAX=PSPOW(48)
      DO 6 I=1,48
6     PSPOW(I)=PSPOW(I)/PSPOW(48)
      INIT=1
100   CONTINUE
C     CHOOSE SPATIAL GROUP
      P=FLTRNF(0)
      DO 7 I=1,48
      IF (P.LE.PSPOW(I)) GO TO 8
7     CONTINUE
8     Z=RAD(I)
C     ASSIGN WATE
      WATE=EXP(+(RCORE-RAD(I))*SIGT)*(EPSMAX/PSMAX)*WATE
C     CHOOSE ENERGY GROUP
      IF(ISOUR) 15,15,60
15    WATE=WATE*DDF
      IF(ISBIAS) 20,20,25
20    NWT=2*NMTG
      GO TO 30
```

```
25    NWT=3*NMTG
30    R=FLTRNF(R)
      DO 35 I=1,NGPQT3
      IF (R- WTS(I+NWT)) 40,40,35
35    CONTINUE
40    IG=I
      IF(ISBIAS) 60,60,45
45    IF(I-1) 60,50,55
50    WATE=WATE*WTS(2*NMTG+1)/WTS(3*NMTG+1)
      GO TO 60
55    WATE=WATE*(WTS(2*NMTG+I)-WTS(2*NMTG+I-1))/
     1(WTS(3*NMTG+I)-WTS(3*NMTG+I-1))
60    CONTINUE
      IF (MRVISO-1) 61,62,61
62    CONTINUE
C     SELECT DIRECTION COSINES
2000  R1=FLTRNF(R)
      R2=FLTRNF(R)
      X1=2.0*R1-1.0
      XSQ=X1*X1
      YSQ=R2*R2
      D=XSQ+YSO
      IF(D-1.0) 2010,2010,2000
2010  COFI=(XSQ-YSQ)/D
      SIFI=2.*X1*R2/D
      R1=FLTRNF(R)
      R2=FLTRNF(R)
      IF(R1-FREQ) 2030,2020,2020
2020  W=CTHETA+(1.0-CTHETA)*R2
      AWATE=0.5*(1.0-CTHETA)*(1.0+BF)/BF
      GO TO 2040
2030  W=(1.0+CTHETA)*R2-1.0
      AWATE=0.5*(1.0+CTHETA)*(1.+BF)
2040  SITH=SQRT(1.0-W*W)
      U=SITH*COFI
      V=SITH*SIFI
      WATE=WATE*AWATE
61    RETURN
      END
```

```
      SUBROUTINE BDRYX
      COMMON /PDET/ ND,NNE,NE,NT,NA,NRESP,NEX,NEXND,NEND,NDNR,NTNR,NTNE,
     1 NANE,NTNDNR,NTNEND,NANEND,LOCRSP,LOCXD,LOCIB,LOCCO,LOCT,LOCUD,
     2 LOCSD,LOCQE,LOCQT,LOCQTE,LOCQAE,LMAX,EFIRST,EGTOP
      COMMON /NUTRON/ NAME,NAMEX,IG,IGO,NMED,MEDOLD,NREG,U,V,W,UOLD,VOLD
     1 ,WOLD,X,Y,Z,XOLD,YOLD,ZOLD,WATE,OLDWT,WTBC,BLZNT,BLZON,AGE,OLDAGE
      COMMON BC(1)
      DIMENSION NC(1)
      EQUIVALENCE (BC(1),NC(1))
      Z2=0.999*Z
      Z22=1.001*Z
      IA = LOCXD + 3*ND
      DO 10 I=1,ND
      IA = IA + 1
      IF(Z2-BC(IA)) 20,20,10
10    CONTINUE
      GO TO 100
20    IF(Z22-BC(IA)) 30,30,40
30    CONTINUE
      GO TO 100
40    COS=W-1.E-10
      ABC = ABS (COS)
      IF (COS) 50,60,50
 50   IF (ABC-1.0001) 70,60,60
 60   CALL HELP (4HBDRX,1,1,1,1)
      CALL ERROR
 70   IF (ABC-0.01) 80,90,90
 80   ABC = 0.005
 90   CON = WATE/ABC
      CALL FLUXST(I,IG,CON,AGE,COS,0)
C  * *  SWITCH =  0  -- STORE IN ALL RELEVANT ARRAYS EXCEPT UD
      INN = LOCXD + 6*ND + I
C * *THIS STORE IS IN THE FIRST OF THE NEXND ARRAYS SET ASIDE BY SCORIN
      NC(INN) = NC(INN) + 1
100   CONTINUE
      ZABS=ABS(Z)
      IF(ZABS-0.001) 1,2,2
1     CALL ALBDO(IG,U,V,W,WATE,NMED,NREG)
2     CONTINUE
      RETURN
      END
```

Appendix III

```
SUBROUTINE GTMED (MDGEOM,MDXSEC)
MDXSEC=(3*MDGEOM)/2-((MDGEOM/2)*2)
IF(MDGEOM.EQ.1000) MDXSEC=1000
RETURN
END
```